Forced tidal response in the Gulf of Mexico

Flavien Gouillon,[1] Steven L. Morey,[1] Dmitry S. Dukhovskoy,[1] and James J. O'Brien[1]

Received 14 January 2010; revised 5 May 2010; accepted 19 May 2010; published 23 October 2010.

[1] This study investigates the characteristics of tides in the Gulf of Mexico (GoM) and the response to forcing by local tidal potential and tides propagating as waves through straits connecting this semienclosed sea to the Caribbean Sea and Atlantic Ocean. Numerical simulations performed with the Navy Coastal Ocean Model run in a barotropic configuration with 1/60° horizontal resolution are used to analyze the tidal response to different forcing mechanisms. The tidal energy budget and tidal energy fluxes in the GoM are calculated from the simulations. Results show that diurnal tides in the GoM are dominantly due to co-oscillation with the western Atlantic and that a substantial amount of semidiurnal tidal energy also enters the Gulf through the straits. Model experiments suggest that adding the local tidal potential significantly modifies the propagation of the semidiurnal tidal signal within the GoM and reduces the tidal power associated with the diurnal tides in the basin. An interesting phenomenon of nonlinear interaction between the two forcing mechanisms (local forcing and propagation through the straits) is described and explained by using a mechanistic mass-spring system model.

Citation: Gouillon, F., S. L. Morey, D. S. Dukhovskoy, and J. J. O'Brien (2010), Forced tidal response in the Gulf of Mexico, *J. Geophys. Res.*, *115*, C10050, doi:10.1029/2010JC006122.

1. Introduction

[2] The tidal regime of the Gulf of Mexico (GoM) has been the subject of several numerical studies. The first attempt to model tides in the GoM was a theoretical work done by *Grace* [1932], who found that the diurnal tides co-oscillate through the Yucatan Channel (YC) and the Straits of Florida (SoF). Further study of GoM tides has been conducted by *Marmer* [1954] and *Zetler and Hansen* [1971], which led to descriptions of the structure of tidal phases around the basin, including the presence of a semidiurnal M2 amphidromic point near the YC. The latter study also found that the M2 semidiurnal and diurnal K1 energy available in the GoM was approximately 2×10^{10} J s^{-1}, comparable to the 3×10^{10} J s^{-1} found by *Miller* [1966]. *Mikhailov* [1969] was the first to model the semidiurnal tides using a numerical solution of the Helmholtz equation. However, this method failed to accurately represent the diurnal tides as their periods were too close to the inertial period within the latitude range of the GoM. A time-marching numerical solution of the primitive equations was then applied to avoid the above problem [*Grijalva*, 1971; *Mungall et al.*, 1978]. Continuing the work done by *Grace* [1932], *Grijalva* [1971] was the first to include direct forcing of the GoM via astronomical forcing, or local tidal potential (LTP), in addition to the usual port condition, or open boundaries (OB). In numerical models, this OB forcing has usually been implemented at the YC and at the SoF, through which the GoM communicates with the Atlantic Ocean. *Mungall* [1978] achieved similar results by tuning a model's OB conditions to match observations (i.e., an inverse modeling method). These authors obtained a reasonable agreement for the diurnal component of tides, but the semidiurnal simulations were not in agreement with observations. *Schwiderski* [1979, 1980] employed the same time-marching method with more accurate tuning at the port and found some significant improvement of the representation of the tidal signal in a high-resolution (1° × 1° was the optimum resolution at the time) model with a GoM configuration. *Reid and Whitaker* [1981] (hereafter, Reid and Whitaker), in an insightful technical report, showed that the primary driving force of the M2 tide is the LTP (55% of the M2 energy) that produces a quasi-resonant, cyclonically rotating shelf wave response with the largest amplitude near Cedar key on the West Florida Shelf (WFS hereafter) and secondary maxima near Galveston, TX, and in the Bay of Campeche. This local amplification is due to tidal resonance across the wide shelf [*Clarke and Battisti*, 1981; *Clarke*, 1995]. Reid and Whitaker also stated that 83% of the variance of the diurnal tidal constituents is owed to phase locking with the port condition. *Kantha* [2005] stated that, in the GoM, astronomical forces are more important for locally generating the semidiurnal tides than the North Atlantic Ocean tidal signal radiating through the SoF and the YC. However, none of the above studies has attempted to isolate the role that LTP plays in affecting the behavior of the propagating tides in the GoM and how it modifies the amplitudes, phases, and energy of the remote tidal signal coming from the Atlantic.

[3] Numerical experiments using a nonassimilative ocean model, described in section 2, are used to understand the

[1]Center for Ocean Atmospheric Prediction Studies, Florida State University, Tallahassee, Florida, USA.

0148-0227/10/2010JC006122

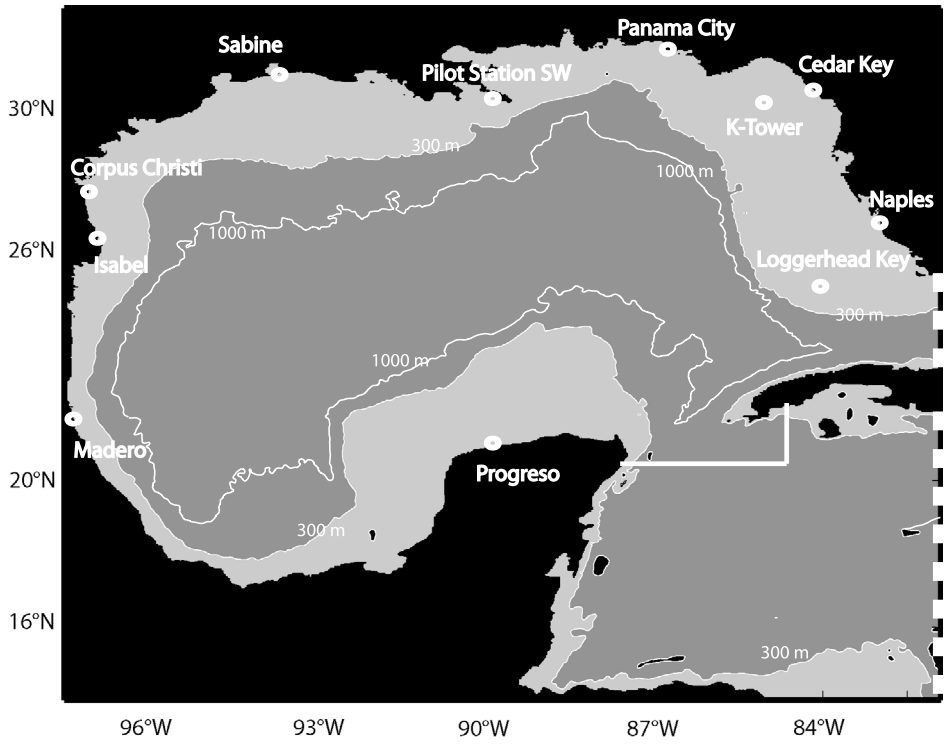

Figure 1. Map of the model domain. The locations of 11 select observational locations used in this study are shown by white circles. Isobaths within the GoM are drawn at 300 and 1000 m. The solid white line delimits the GoM region used for energy computations, and the dashed line shows the model open boundaries along the eastern edge.

nature of tides in the GoM and their relation to tidal forcing. A set of experiments is conducted to yield new understanding of the tidal response due to the LTP, tidal signal propagation through the straits connecting the GoM to the Atlantic by considering forcing at the model OB, and the modification of the propagating tidal signal by combining both model forcing mechanisms. In section 3, a comparison of the model results with observations and previous studies is presented. Section 4 presents estimates of the total tidal energy, tidal budget, and tidal energy fluxes for the semidiurnal and diurnal constituents produced from the model.

2. Model and Experiment Setup

[4] In this study, the Navy Coastal Ocean Model (NCOM) [*Martin*, 2000] is applied to simulate the barotropic response of the GoM to tidal forcing. The NCOM is a three-dimensional ocean model with a hybrid sigma (or terrain following)/*z* level (or geopotential following) vertical coordinate system that can be configured by the user with great flexibility. It has a free surface and is based on the primitive equations with hydrostatic, Boussinesq, and incompressibility approximations. The model uses an Arakawa C staggered grid and is leapfrog in time with an Asselin filter [*Asselin*, 1972] (with a coefficient of 0.05) to suppress computational modes associated with time splitting, and the application presented here uses second-order centered spatial finite differences. In these simulations, the NCOM is run with one sigma layer and homogeneous temperature and salinity fields resulting in a barotropic configuration of the model. The bottom friction used in these simulations is parameterized with a quadratic drag law and implicitly calculated by the model. The drag coefficient c_b is calculated as

$$c_b = \max\left\{\frac{K^2}{\ln^2\left(\frac{\Delta z_b}{2z_0}\right)}, c_b \min\right\}, \quad (1)$$

where K is the Von Karman constant, cbmin is the minimum value that the bottom drag coefficient can attain (set at 0.0025 in this study), Δz_b is the height of the bottom grid cell (in a barotropic model this corresponds to the total water column depth), and z_0 is the bottom roughness (in this study z_0 = 3 mm). For this barotropic simulation, it is simple to show that for regions with the seafloor depth greater than approximately 17 m, cb will take on its minimum value of 0.0025.

[5] The model domain has a horizontal grid with dimensions 1040 × 944 that encompasses 98.15°W–80.60°W, 15.55°N–31.50°N (Figure 1). The horizontal resolution is 1/60°, and the model time step is 240 s. Model OB are in the SoF and the Caribbean Sea (dashed line at the eastern edge of the map in Figure 1), and *Flather* [1976] OB conditions are applied. The basin is initially at rest, and in these simulations, there is no forcing but the tidal forcing, which is detailed later. The simulations run with this model configuration do not assimilate data, as is typically done in numerical models designed to produce accurate

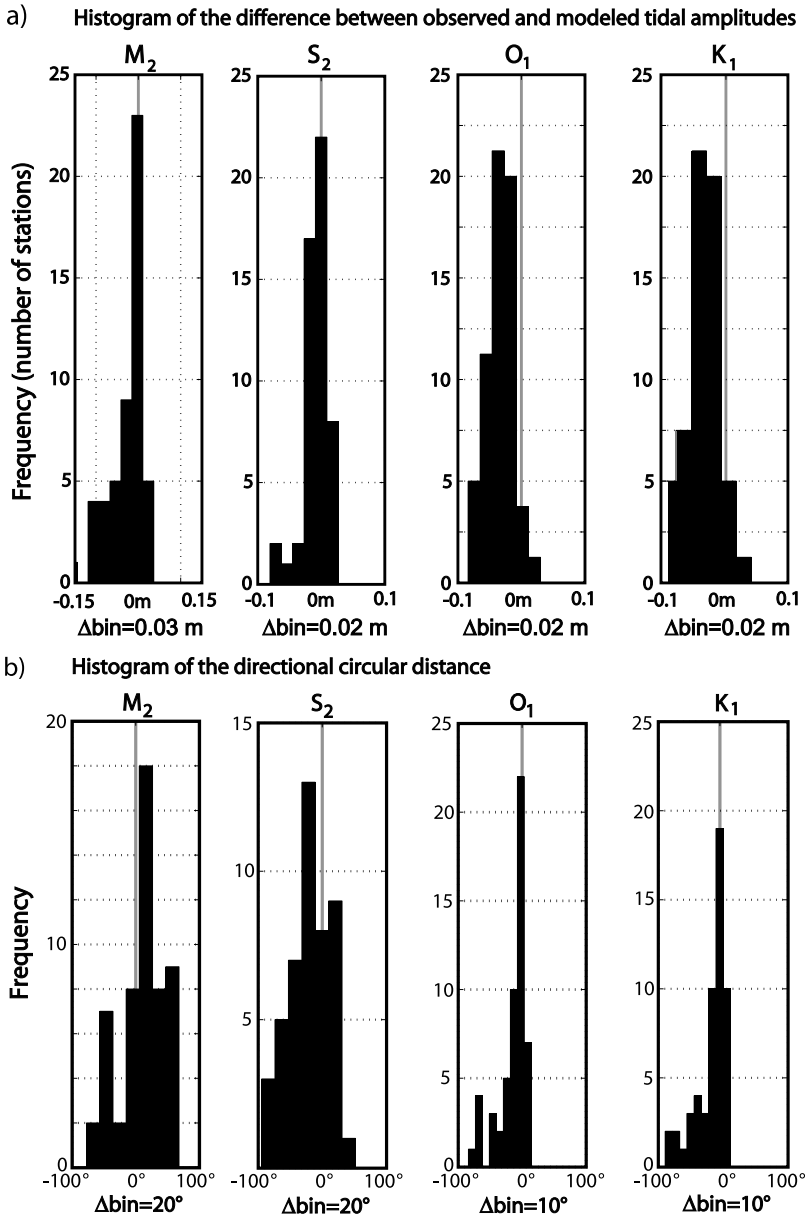

Figure 2. Histograms of (a) the difference between the observed and modeled tidal amplitudes (observed-model) for constituents M_2, S_2, O_1, and K_1 and (b) the directional circular distance.

tidal predictions. The purpose of assimilating data (typically coastal sea level observations from tidal stations) is to adjust the model to correct for errors in the local tidal amplitudes and phases that arise due to irresolvable topography and coastline geometry and poorly known parameterizations for processes such as tidal energy conversion and dissipation due to bottom friction. However, the purpose of this study is not only to produce a tidal simulation for the region but also to investigate the dynamical response of propagating tidal signals in the basin as free waves co-oscillating with the western Atlantic Ocean, as well as the modification of the remotely generated tidal signals by local forcing. Thus, it is useful for this study to not constrain the model solution by data assimilation but rather to produce realistically simulated tides through accurate forcing mechanisms using a very fine resolution model grid.

[6] Model output is analyzed beginning at the fourth day of the model integration when the basin-integrated tidal energy oscillates about an equilibrium state (this behavior is evident after approximately 40 h of model integration). The use of a semi-implicit time-differencing scheme allows the model to remain numerically stable for time steps that exceed that required by the Courant-Friedrichs-Lewy condition. Sensitivity tests on the model time step show that phase errors arising from the choice of time step are negligibly small (nearly nondetectable), as was also found in a modeling study with similar dynamics by *Henson et al.* [2006]. Model variables are saved at hourly intervals for analysis.

Table 1. Tidal Station Information[a]

Station	NOAA ID	Longitude	Latitude
Loggerhead Key	8724698	82°55.2′W	24°37.9′N
Vaca Key	8723970	81°06.3′W	24°42.7′N
Key West	8724580	81°48.5′W	24°33.2′N
Fort Myers	8725520	81°52.3′W	26°38.8′N
Port Manatee	8726384	82°33.9′W	27°38.2′N
Clearwater	8726724	82°49.9′W	27°58.7′N
Johns Island	8727235	82°38.3′W	28°41.5′N
Shell Island	8727359	82°41.5′W	28°55.4′N
St. Marks Lighthouse	8728130	84°10.7′W	30°04.7′N
Turkey Point	8728360	84°30.7′W	29°54.9′N
Apalachicola	8728690	84°58.9′W	29°43.6′N
Panama City	8729108	85°40.0′W	30°09.1′N
Navarre Beach	8729678	86°51.9′W	30°22.6′N
Pensacola	8729840	87°12.7′W	30°24.2′N
Dauphin Island Hydro	8735180	88°04.5′W	30°15.0′N
Horn Island, MS	8742221	88°40.0′W	30°14.3′N
Gulfport Harbor	8745557	89°04.9′W	30°21.6′N
Waveland	8747437	89°22.0′W	30°16.9′N
South Pass	8760551	89°08.4′W	28°59.4′N
Grand Isle	8761720	89°58.1′W	29°15.3′N
Port Fourchon	8762075	90°12.0′W	29°06.9′N
Eugene Island	8764311	91°23.1′W	29°22.3′N
Freshwater Canal Locks	8766072	92°18.3′W	29°33.3′N
Calcasieu	8768094	93°20.6′W	29°45.9′N
Sabine offshore	8771081	93°38.4′W	29°29.9′N
Rollover Pass	8770971	94°30.8′W	29°30.9″N
Galveston	8771510	94°47.3′W	29°17.1’ N
USCG Freeport	8772447	95°18.0′W	28°56.0′N
Port O’Connor	8773701	96°23.3′W	28°27.1′N
Port Aransas, Caldwell Pier	8775237	97°03.0′W	27°49.6′N
Packery Channel	8775792	97°14.2′W	27°38.0′N
Corpus Christi	8775870	97°13.0′W	27°34.8′N
Padre Island	8779750	97°09.4′W	26°04.1′N
Madero, Tampico	9500966	97°47.7′W	22°15.7′N
Naples	8725110	81°48.4′W	26°07.8′N
St. Petersburg	8726520	82°37.5′W	27°45.5′N
Tuckers Island	8727277	82°41.7′W	28°46.3′N
Mangrove Point	8727333	82°43.4′W	28°52.2′N
Ozello North	8727306	82°40.0′W	28°51.8′N
Cedar Key	8727520	83°01.9′W	29°08.1′N
Shell Point	8728229	84°17.4′W	30°03.6′N
Weeks Bay	8732828	87°49.5′W	30°25.0′N
Pascagoula Point	8741196	88°32.0′W	30°20.4′N
Coast Guard sector Mobile	8736897	88°03.5′W	30°38.9′N
Biloxi	8744117	88°54.2′W	30°24.7′N
Bay Waveland Yacht club	8747437	89°19.5′W	30°19.5′N
Shell Beach	8761305	89°40.4′W	29°52.1′N
South West Pass	8760943	89°25.0′W	28°55.5′N
Texaco Dock	8761819	90°02.3′W	29°24.1′N
Lawma, Amerada Pass	8764227	91°20.4′W	29°27.0′N
Cypremort Point	8765251	91°52.8′W	29°42.8′N
Galveston Bay entrance	8771341	94°43.5′W	29°21.5′N
Port Ingleside, Corpus Christi Bay	8775283	97°12.2′W	27°49.3′N
Port Isabel	8779770	97°12.9′W	26°03.6′N
Tampico, TAMPS, Madero	/	97°51.3′W	22°13.0′N
Tuxpan, Ver.	/	97°20.0′W	21°00.0′N
Veracruz, Ver.	/	96°08.2′W	19°12.1′N
Alvarado, Ver.	/	95°45.9′W	18°46.7′N
Coatzacoalcos, Ver.	/	94°24.7′W	18°08.9′N
Ciudad del Carmen, Camp	/	91°50.3′W	18°32.4′N
Progreso, Yucatan	/	89°39.5′W	21°18.0′N
K-Tower (N7)	/	84°22.2′W	29°40.0′N

[a]Stations that are considered as outliers for the M2 tidal amplitude using the Studentized test are shown in bold.

[7] To analyze the tidal response within the GoM to different forcing mechanisms, three model experiments are performed. Each numerical experiment is integrated for a period of 1 month. In the first experiment, the model is forced with LTP at each grid point (LTP experiment). This LTP is computed from Newton’s theory of equilibrium tides given in the study by *Mellor* [1996] as

$$\eta_{\mathrm{eq}}(\lambda,\varphi,t) = \cos^2\varphi \sum_i A_i \cos(\omega_i t + \chi_i + 2\lambda) + \sin(2\varphi) \sum_j A_j \cos\left(\omega_j t + \chi_j + 2\lambda\right). \quad (2)$$

The following notation has been used in the above equation: η denotes the surface elevation, A is the amplitude, ω is the frequency, ϕ is the latitude, λ is the longitude, χ is the phase at time t, i is a specific semidiurnal constituent, and j is a specific diurnal constituent (the term representing the long-period tides is not included here). The LTP forcing is then only dependent on the amplitude, phase, and frequency of the tidal constituent, the latitude and longitude of the location considered, and the time. The horizontal gradient of this term representing the equilibrium tidal elevation is then incorporated into the primitive equations.

[8] In the second experiment, the tidal forcing is implemented by specifying the elevation and barotropic transport for each tidal constituent at the model open boundaries, derived from the U. S. Army Corp of Engineers ADCIRC East Coast Tide model [*Mukai et al.*, 2002]. This tidal model, based on an unstructured-grid barotropic ocean model, provides estimates of tidal amplitude and phase for the Atlantic Ocean, Caribbean Sea, and GoM west of 60°W. It is forced with astronomical forcing and boundary conditions derived from the *Le Provost et al*. [1998] global tidal model. Extensive comparisons to tidal observations by *Mukai et al*. [2002] demonstrate that these model estimates are sufficiently accurate in the vicinity of the GoM model OB for the purposes of this study. Errors that arise from application of the ADCIRC tidal estimates at the OB are discussed further in section 3.2. This experiment is referred to as the OB experiment and is only forced by the tidal signal passing between the GoM and the Atlantic through the SoF and the Caribbean Sea.

[9] The third experiment combines the LTP and OB forcing mechanisms as described above and produces the most realistic simulation of tides in the GoM of any of the three experiments. This is referred to as the LTP and OB experiment.

[10] For each of the model experiments, only the M_2, S_2, O_1, and K_1 tidal constituents are included in the simulations, as these are the dominant semidiurnal and diurnal tidal constituents in the GoM. These four tidal constituents represent 90% of the tidal bulk in the GoM [*He and Weisberg*, 2002]. The semidiurnal M_2 and S_2 constituents have periods of 12.421 and 12.00 h, respectively, and the O_1 and K_1 constituents have periods of 25.82 and 23.93 h, respectively.

3. Tidal Phases and Amplitudes

3.1. Model Validation

[11] To validate the model solution for the tides in the region, the tidal phases and amplitudes from 62 tidal stations (55 operated by the National Oceanic and Atmospheric Administration or academic institutions, including stations used by *Reid and Whitaker* [1981], as well as seven Mexican tidal stations [*Servicio del Golfo de Mexico y Mar Caribe*, 2007]) are compared to the model tidal estimates

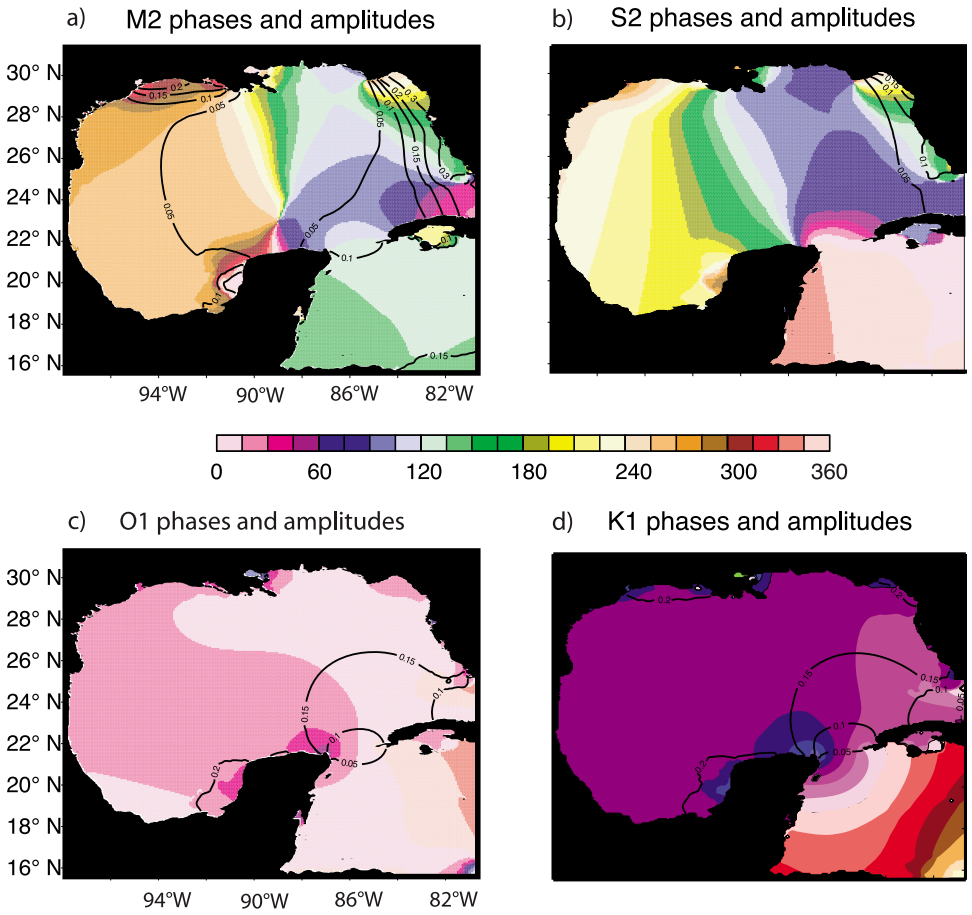

Figure 3. Tidal phases (in degrees) and amplitudes (meters) calculated from the LTP and OB model experiment for each of the four tidal constituents considered in this study: (a) M_2, (b) S_2, (c) O_1, and (d) K_1. Phases are shaded with a periodic color map. Amplitudes are contoured with a 0.05 m interval.

calculated from the LTP and OB experiment. At every model grid point, the sea surface elevation time series from the model is analyzed using the T-Tide [*Pawlowicz et al*, 2002] harmonic analysis utility to extract estimates of the phase and amplitude. It is necessary to point out that some of these stations are located near complex coastline geometry, e.g., in bays or behind islands that are not resolved in the model. Thus, discrepancies between the model and the observed tidal amplitudes and tidal phases for such stations are anticipated. Visual inspection of histograms of the differences between observed and modeled amplitudes for the four tidal constituents (Figure 2a) suggests that the model tends to slightly overestimate the amplitudes of all the tidal constituents. This could be explained by errors in prescribing the model open boundaries, or by insufficient dissipation of tidal energy within the basin.

[12] For the semidiurnal tides, the root-mean-square errors computed across the observation locations are 0.045 m for M_2 and 0.018 m for S_2. A studentized residual analysis (Appendix A) is applied to objectively identify outliers for the model-data comparisons. These outliers include Packery Channel (North Corpus Christi), St. Petersburg, and Ozello North for the semidiurnal tides. Inspection of the local geography about each of these stations shows that they are located in areas of unresolved complicated coastline geometry where the model is unable to simulate accurately the tidal propagation. These tidal stations are located behind islands (i.e., Packery Channel, Ozello North) or in bays (i.e., St. Petersburg), which strongly modify the local tidal signal (see Table 1 for tidal station location information). After deleting these outliers, the correlation between the simulated and observed amplitudes is 0.88 for M_2 and 0.91 for S_2.

[13] The correlation analysis of the diurnal tide is not useful because the amplitudes and phases of the diurnal constituents vary little spatially over the GoM away from bays due to the co-oscillating phenomena (as can be seen in Figures 3c–3d). Thus, even relatively small deviations from the observed values of the simulated amplitude or phase will result in low correlation coefficients. At the locations of some tidal stations, the amplitude is strongly modified locally due to shallow bays or islands unresolved by the model, which will dramatically reduce the correlation between the observed and modeled amplitudes. Thus, this statistical approach is not applied for the diurnal constituents. The root-mean-square errors for amplitudes of the diurnal constituents are 0.026 m for O_1 and 0.034 m for K_1.

[14] Histograms of the directional circular distance (absolute value of the phase difference) (Figure 2b) show that the phase differences between the model and observations at the 62 stations are clustered about zero. For the semidiurnal constituents, there are several locations where the simulated phase differs by as much as 90° from the

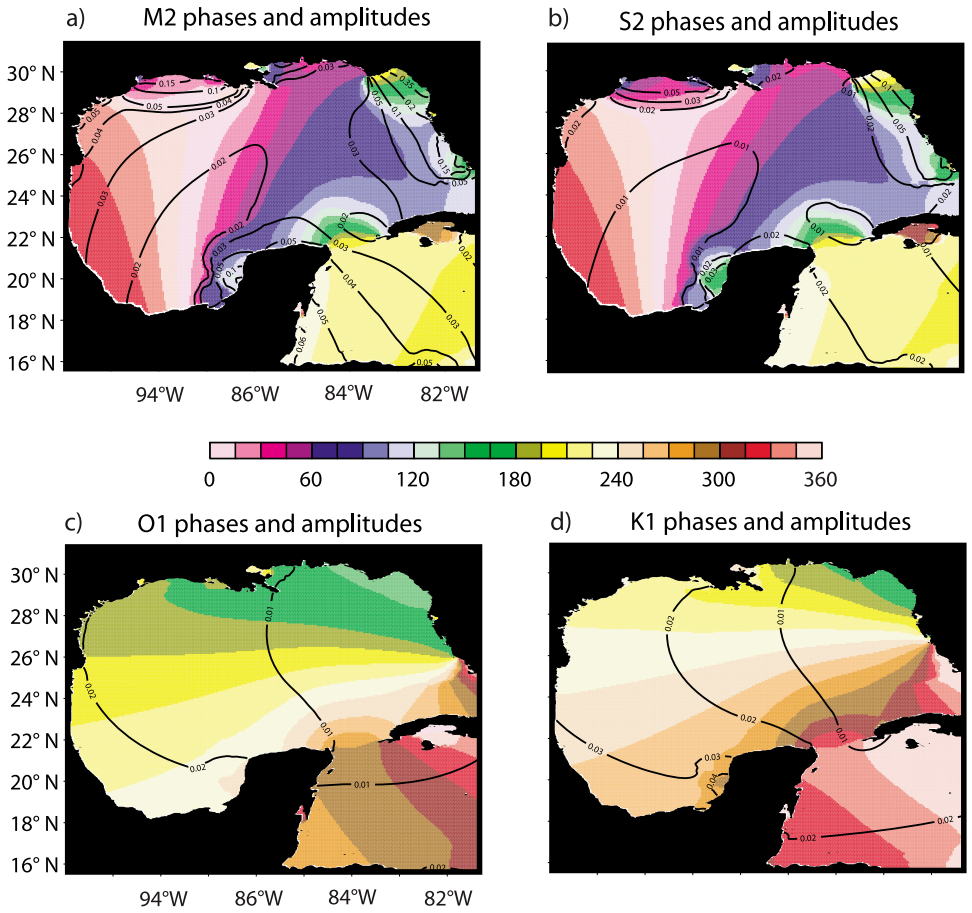

Figure 4. Tidal phases (in degrees) and amplitudes (meters) calculated from the LTP model experiment for each of the four tidal constituents considered in this study: (a) M_2, (b) S_2, (c) O_1, and (d) K_1. Phases are shaded with a periodic color map. Amplitudes are contoured with a 0.05 m interval.

observed phase. These differences might be explained by inaccuracies in the model bathymetry near the coastal areas where these tidal gauges are located or by inaccurate parameterization of the bottom friction in shallow regions. There is also a slight phase error in the data prescribed at the model open boundaries as is discussed later in this section.

[15] To estimate the relation between observed and simulated tidal phases, which are circular data, the circular correlation coefficients are calculated following *Jammalamadaka and Sarma* [1988]. For the semidiurnal constituents, those are given by

$$\rho_c(\alpha,\beta) = \frac{\mathrm{E}\{\sin(\alpha-\mu)\sin(\beta-\upsilon)\}}{\sqrt{\mathrm{var}(\sin(\alpha-\upsilon))\mathrm{var}(\sin(\beta-\upsilon))}}, \qquad (3)$$

where α and μ are the model phase and mean phase, respectively, and β and υ are the observed phase and mean phase. The circular correlation coefficient ρc for the M_2 tidal constituent is 0.84 and for the S_2 tide is 0.71. The circular correlation coefficient computation is not applied for the diurnal tidal phases because of their low spatial variability, similar to the low spatial variability of the diurnal tidal amplitudes as discussed above.

[16] This statistical validation approach shows that errors for the simulated tidal amplitudes and phases are comparable to what is commonly expected using such a model configuration [*Blanton et al*, 2004], smaller than earlier, coarser-resolution studies [e.g., *Reid and Whitaker*, 1981], and comparable to more recent studies in the GoM [*He and Weisberg*, 2002]. Thus, the model can be used with confidence for additional model experiments and analyses for studies of the behavior of tides in the basin. Additionally, the preceding validation defines limitations in the model performance in certain coastal areas, so that local coastal geometry and bathymetry can be considered when selecting tidal stations for analyzing additional experiments in the next section.

3.2. Model Experiments

[17] Maps of the phase lag and amplitudes for each tidal constituent are produced from the numerical experiments. Examining the LTP and OB experiment, which is the most realistic simulation, the semidiurnal M_2 constituent (Figure 3a) has an amphidromic point north of the Yucatan Peninsula (YP) in good agreement with previous modeling studies by *Kantha* [2005]. There is no amphidromic point for the S_2 constituent, as the co-tidal lines seem to converge near the YP (Figure 3b). The co-tidal lines become compacted in the central GoM, roughly following a line from the central U. S. Gulf Coast to the YP, showing that the semidiurnal tidal

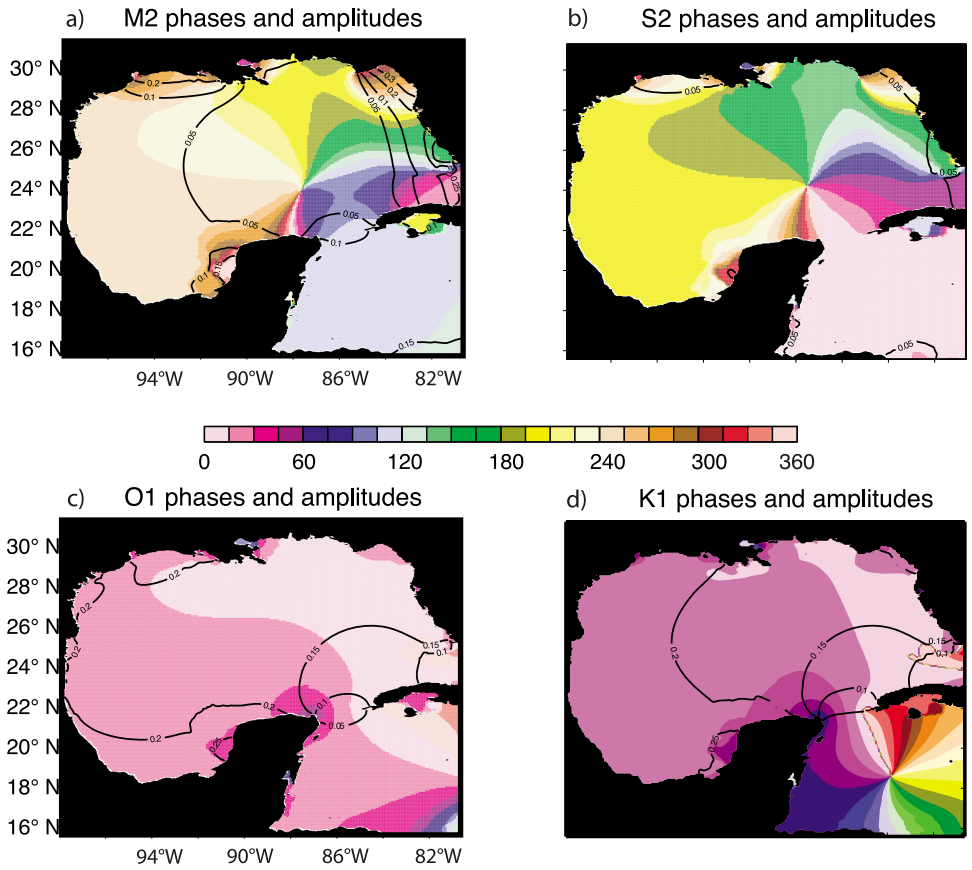

Figure 5. Tidal phases (in degrees) and amplitudes (meters) calculated from the OB model experiment for each of the four tidal constituents considered in this study: (a) M_2, (b) S_2, (c) O_1, and (d) K_1. Phases are shaded with a periodic color map. Amplitudes are contoured with a 0.05 m interval.

propagation slows down near this region. This region demarcates a change in the tidal pattern in the GoM, as the western part of the basin is dominated by diurnal energy and semidiurnal tides dominate on the shelf in the east [*Zetler and Hensen*, 1971]. In the western part of the basin, the M_2 tide phase is rather spatially uniform. The maximal simulated tidal amplitudes occur in coastal areas with wide shelves, particularly near Cedar Key and near the Louisiana-Texas coastline where the amplitude reaches nearly 0.4 m. The tidal amplification at these locations can be explained by the near resonance of this period of oscillation across the wide shelves [*Clarke*, 1995].

[18] The results considering only astronomical forces are studied using the LTP experiment. The co-tidal lines show the propagation of the perturbation generated locally in the model domain by the LTP forcing. This perturbation travels as a forced wave, and the signal propagates primarily westward (Figure 4). The semidiurnal tidal amplitudes, when forced only by the LTP, are very small in the deep interior basin but are amplified from 10 to 35 cm in coastal areas proximate to wide shelves.

[19] When one considers only the OB forcing, the amplitudes of the semidiurnal tidal constituents are similar to the results from the most realistic LTP and OB model experiment. The amphidromic point for the M_2 constituent (Figure 5a) is slightly shifted to the northeast compared to the LTP and OB experiment (Figure 3a). An amphidromic point appears for the S_2 tide near the M_2 amphidromic point (Figure 5b); this amphidrome does not exist in the realistic case (Figure 3b).

[20] In this OB experiment, the tide propagates as a free wave, as it is not forced by the LTP. The spacing of the co-tidal lines suggests that the propagation of the semidiurnal tide is faster in this simulation in the central part of the GoM and slower in the eastern Gulf than simulated by the LTP and OB experiment. This suggests that modification of the waveform by the addition of LTP forcing acts to retard (in the central Gulf) or accelerate (in the eastern Gulf) the apparent tidal propagation.

[21] For the diurnal tides simulated in the realistic LTP and OB experiment, the patterns for the amplitudes and phases are also generally in agreement with previous modeling studies [e.g., *Kantha*, 2005]. The amplitudes and phases are nearly spatially homogeneous over the basin (Figures 3c–3d). For both diurnal constituents, the amplitude is generally between 10 and 20 cm within the model domain. The spatially nearly homogeneous behavior of the diurnal tides is consistent with the well-known co-oscillating phenomenon in the GoM [*Grace*, 1932]. The tidal signals with similar phases at the YC and SoF cause resonance due to the geometry of the GoM and its natural periodicity.

[22] Considering only tidal forcing at the OB for diurnal constituents (Figures 5c and 5d), the amplitudes and phases are very similar to the LTP and OB results (Figures 4c

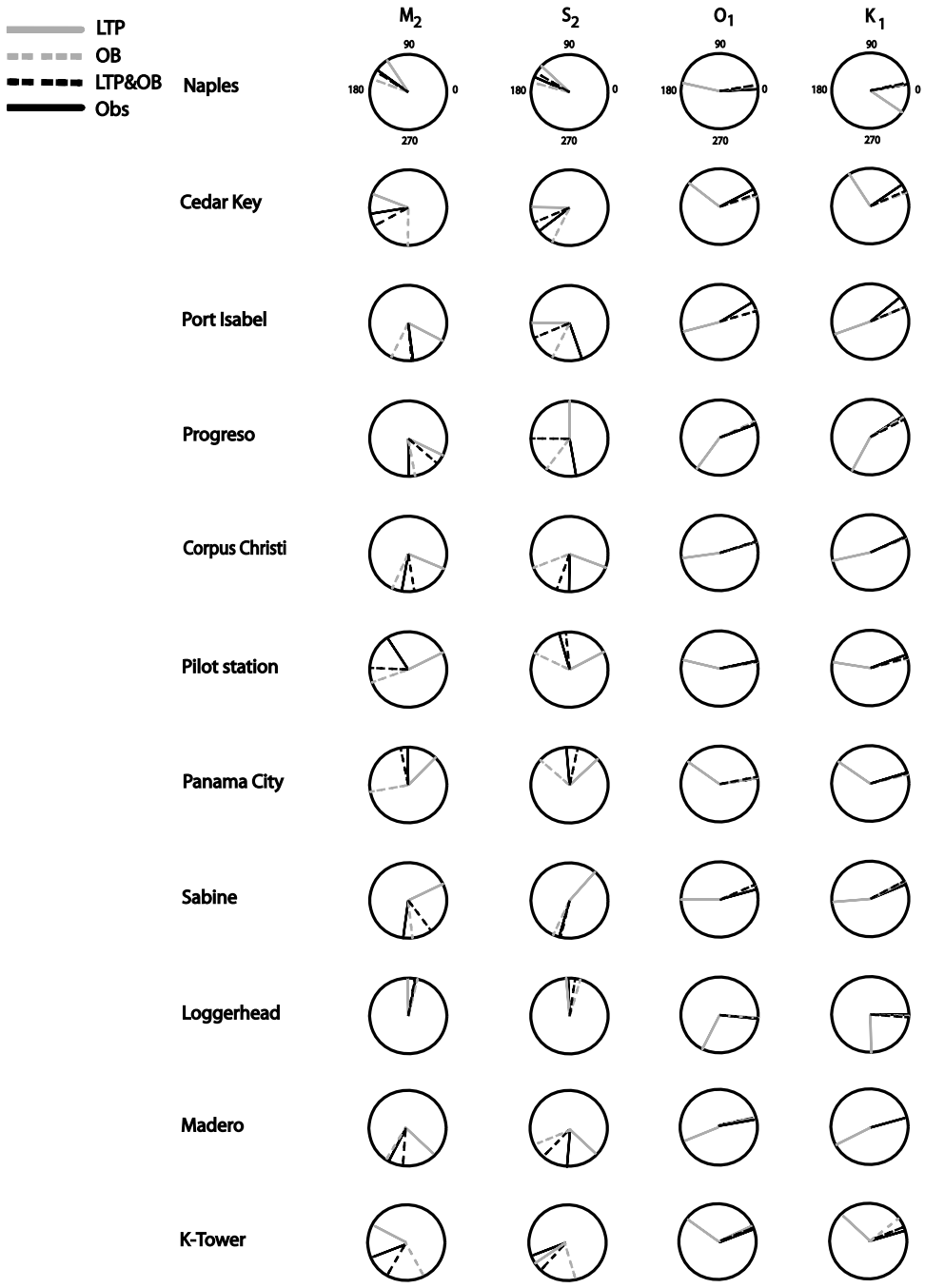

Figure 6. Tidal phases for each tidal station shown in Figure 1 (in rows) and each tidal constituent (in columns). Phases are in degrees and are represented on a circle in the mathematical sense. Line styles correspond to the different model experiments and are defined in the legend in the upper left. In cases where OB and LTP and OB results are nearly identical, only the phase from the LTP and OB experiment is shown.

and 4d). Amplitude magnitudes are somewhat higher in the western part of the basin (5 cm) for the K_1 constituent and change little for the O_1 tides. The tidal amplitudes due to only astronomical (LTP) forcing are very weak and do not exceed 0.04 m (Figures 4c and 4d). These results imply that the LTP is not a major contributor of diurnal tidal energy in the GoM. The diurnal tides are dominated by the tidal signals radiating from the OB, which confirms previous studies [*Zetler and Hensen*, 1971; *Reid and Whitaker*, 1981; *Kantha*, 2005].

[23] Simulated phases and amplitudes of the four tidal constituents are compared with observations at select stations to further understand the behavior of the tides in each of the model experiments (Figures 6 and 7). Following the analysis of section 3.1, these stations are chosen carefully such that they are on relatively straight coastlines facing

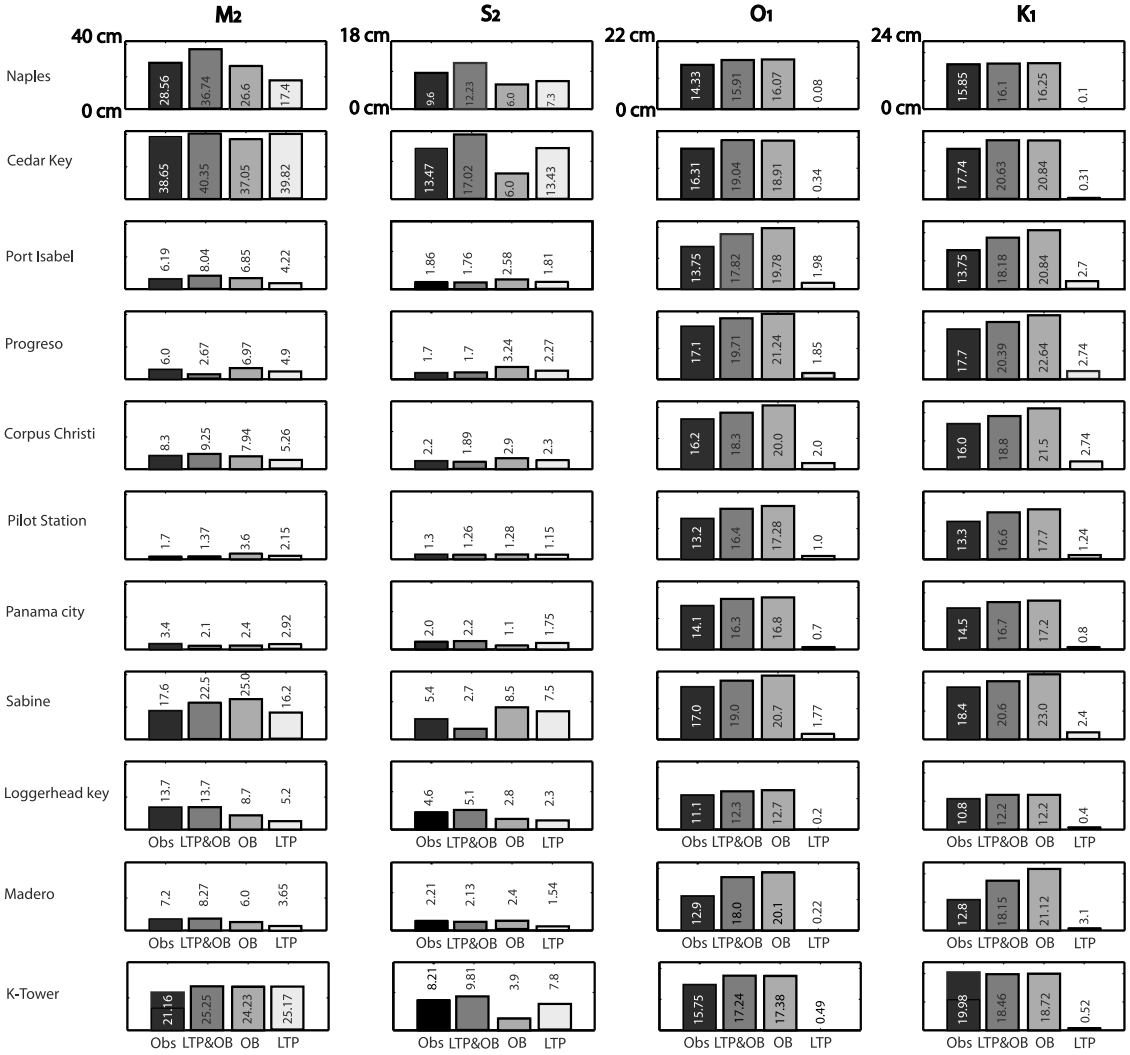

Figure 7. Tidal amplitudes for each tidal station shown in Figure 1 and each tidal constituent (in cm). Note that the scale changes for each tidal constituent.

open water, as significant modification of the tidal propagation and energy can occur around complicated coastline geometry and in bays, which are not well resolved by the model.

[24] The Loggerhead Key tidal station (Figure 1) is very close to the model eastern open boundary at the SoF. Thus, comparison between observed and simulated tidal parameters at this location can be used to verify the open boundary conditions derived from the East Coast ADCIRC tidal model. Phases and amplitudes for the four tidal constituents are in good agreement between the LTP and OB simulation and the values derived from observations at this location (Figures 6 and 7).

[25] Visual inspection of the phases of the semidiurnal constituents (M_2 and S_2, two leftmost columns in Figure 6) reveals that, in most cases, the freely propagating tidal signal generated at the OB alone is not sufficient to provide an accurate model of the semidiurnal tide. Errors in the semidiurnal phases are reduced with the addition of LTP modification of the propagating tidal signal for most of the stations, with exceptions being Progresso, Sabine, Madero, and possibly Corpus Christi. The LTP and OB experiment has a tendency to slightly (~+1.4 cm) overestimate the semidiurnal tidal amplitude compared to the OB forced experiment, with the strongest positive bias in the eastern GoM (Figure 7 and Table 2). The LTP forcing alone also contributes to the tidal bulk but is secondary to the OB forcing.

[26] The phases for O_1 and K_1 signals (Figure 6) show a fairly accurate simulation of the diurnal tides in the model OB and LTP and OB experiments. The largest error in the comparisons between the observed phases and the phases simulated in the LTP and OB experiment is about 15° for Cedar Key and Port Isabel, and the phase errors do not exceed 8° for the other stations. Large phase errors in the LTP experiment are not surprising, as it has already been

Table 2. Mean Deviation From Observations (bias) of Tidal Amplitudes Computed From the Stations Shown in Figure 1

Experiment	M_2	S_2	O_1	K_1
LTP	-0.029	-0.0026	-0.137	-0.139
OB	0.0011	-0.0086	0.0338	0.0378
LTP&OB	0.014	0.0042	0.0241	0.0246

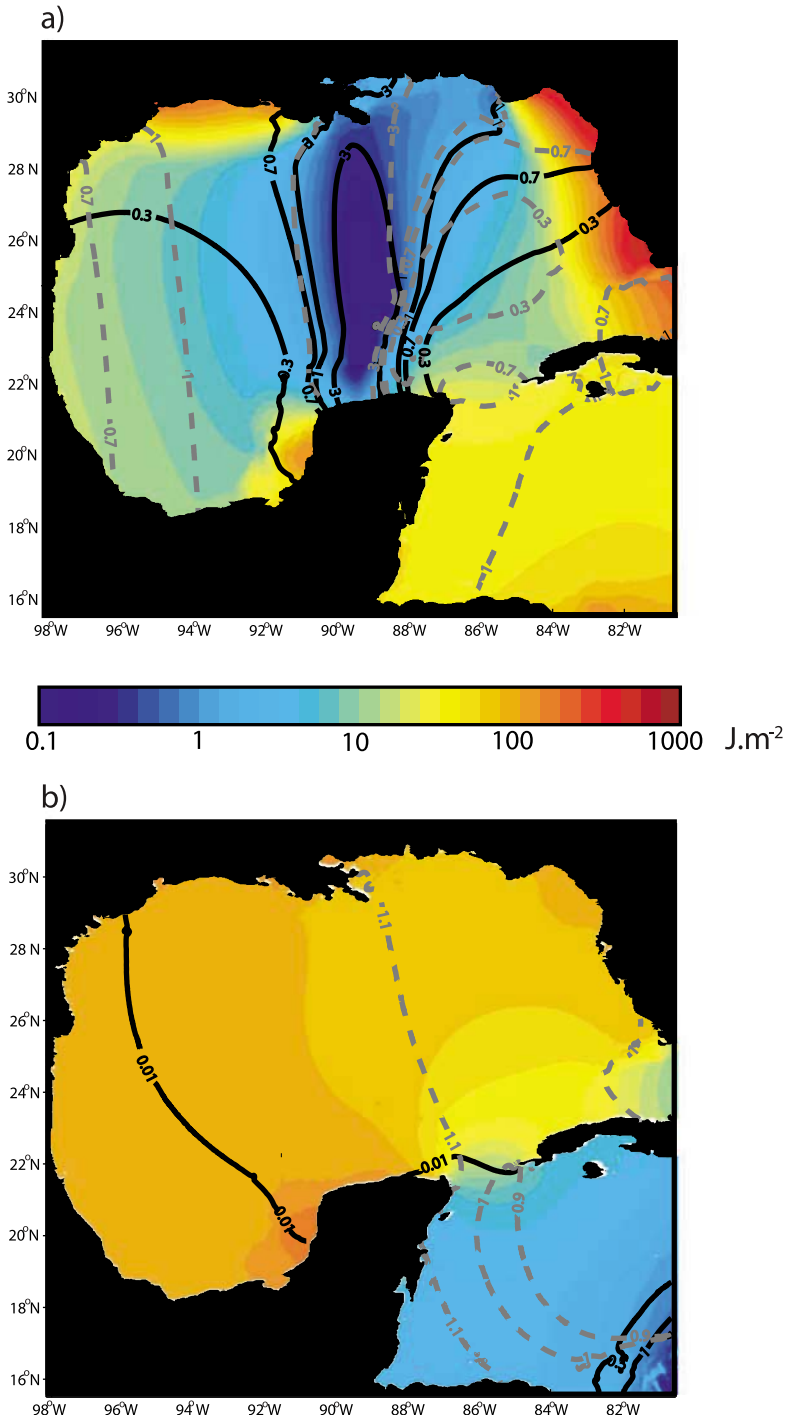

Figure 8. Total (a) M_2 and (b) O_1 tidal energy density in the GoM averaged over a tidal cycle for the LTP and OB model experiment (colored on a logarithmic scale in units of J m^{-2}). Contours are the ratios of the tidal energy density for the LTP experiment (black solid line) or OB experiment (gray dashed line) to the tidal energy density of the LTP and OB model experiment.

established that the local forcing produces only very small diurnal tides in the basin and the diurnal tides are dominantly driven at the open boundary. At all locations, the model amplitudes are slightly greater than observed, with a maximum difference of 0.05 m for the Port Isabel gauge (Figure 7). The modeled amplitude at Loggerhead Key is also greater than observational data suggesting that this may be an impact of inaccuracies in the OB data obtained from the ADCIRC model. Indeed, *Mukai et al*. [2002] show that the ADCIRC model near the GoM boundaries has errors of approximately 8.15% of the observed O_1 tidal amplitude as well as a 3.5° phase shift.

[27] Analyses of these three experiments verify previous suggestions of co-oscillation of the diurnal tides in the basin

Table 3. Tidal Energy in the Gulf of Mexico[a]

Tidal Constituent	LTP and OB	OB	LTP
M_2	77.82	64.42	29.32
O_1	234.42	269.96	1.74

[a]Averaged over a tidal period calculated from the LTP and OB, OB, and LTP model experiments for M_2 and O_1 constituents (measurements are in TJ).

with the western Atlantic and the irrelevance of the LTP for these tidal frequencies. However, the experiments also suggest that the LTP provides not only a nonnegligible contribution to the semidiurnal tidal energy in the GoM but also substantial modification of the incoming M_2 and S_2 tidal signals. These concepts can now be investigated more thoroughly by studying the tidal energetics in the basin with additional model simulations.

4. Tidal Energetics

4.1. Tidal Energy Density

[28] A separate set of model experiments is run to calculate tidal energy density maps, the tidal power, and energy fluxes for the main lunar diurnal (O_1) and semidiurnal (M_2) constituents. The NCOM is configured as before for the LTP and OB, LTP, and OB experiments, but this time forced with only one constituent frequency at a time for each experiment. As mentioned above (in section 2), all computations introduced in this section are done after the model has reached a state of equilibrium. The tidal energy density (U) is calculated as the sum of the kinetic and potential energy per unit area, averaged in time over the tidal period T for the O_1 and M_2 constituents in the experiments considering different tidal forcing mechanisms.

$$U = \frac{1}{T}\left(\int_0^T \frac{\rho D}{2}\left(u^2 + v^2\right)\mathrm{d}t + \int_0^T \rho g D \eta \mathrm{d}t\right), \qquad (4)$$

where D is the total depth; ρ is the density; g is the gravity acceleration; and u, v, and η are the time-dependent tidal velocity components and free surface deviations. From these maps, the tidal energy density excited individually by the LTP forcing and OB forcing over the GoM can be compared.

[29] The prominent feature of the spatial distribution of M_2 tidal energy in the GoM from the LTP and OB experiment is a well-localized minimum in the central GoM, coincident with the amphidromic point, where the tidal amplitude is naturally at a minimum (Figure 8a). The amplification of the tidal energy over the WFS and Texas-Louisiana coast is consistent with the amplification due to resonance across the shelf as described earlier. Contours of the ratios of tidal energy density from the LTP versus LTP and OB experiments and the OB versus LTP and OB experiments show regions where the two forcing mechanisms work constructively together to increase the tidal amplitude, as well as regions where destructive interference occurs (Figure 8). Where both ratios are less than one, the two must necessarily add constructively to increase the tidal amplitude. Regions where one or both ratios are greater than 1 show regions where the local forcing by LTP destructively interferes with the propagating tidal signal. The tidal energy for the O_1 constituent is rather uniformly distributed over much of the GoM, and the ratios of tidal energy between the experiments show that the LTP serves to reduce the diurnal tidal energy throughout the basin (Figure 8b).

[30] The energy density (4) is spatially integrated over the GoM portion of the model domain (delimited by the solid white line near the YC in Figure 1) to compute the total tidal energy within the basin (Table 3). When integrated over the GoM, the LTP contributes 29.32 TJ of tidal energy at the M_2 frequency. When forced only at the open boundaries, the total M_2 tidal energy is 64.42 TJ. In the LTP and OB experiment, the total power is 77.82 TJ. The total tidal energy for the O_1 diurnal tides integrated over the GoM is 269.96 TJ when forced only at the open boundary, reduced to 234.42 TJ with the addition of the LTP (Table 3). The total tidal energy within the GoM (Table 3) illustrates how interference between the freely propagating tide (OB simulation) and LTP forcing alters the tidal energy within the basin.

[31] For M_2, LTP forcing adds to the total energy (constructive interference), but for O_1, LTP forcing reduces the energy (destructive interference). Here interference is considered as the modification of the tidal amplitude due to the freely propagating tide wave (either through the open boundary or at rest in the LTP experiment) by local astronomical gravitational forces. One can notice that, for the O_1 tidal constituent, adding LTP forcing to the OB forced experiment reduces the tidal energy of the system by 35.54 TJ. However, the energy within the GoM when forced by LTP only is 1.74 TJ (Table 3), about 5% of the energy change between the OB and LTP and OB experiment. This shows that the contributions to the tidal energy from the OB and LTP forcing cannot be linearly additive. A cursory explanation might be that the energy is proportional to the square of the tidal amplitude. A simple oscillating spring-mass system can be used to further illustrate this nonlinearity of the contribution of two different forcing mechanisms to the energy budget, following a similar approach to explain tidal resonance in the study by *Arbic and Garrett* [2009].

[32] Consider the classic example of a mass m connected to a spring with spring constant k, damping constant γ, subject to two external forces of amplitudes A_1 and A_2 oscillating with frequency ω, but out of phase by $\delta\phi = \phi 2 - \phi 1$. The displacement x of a unit mass from its equilibrium position at time t (with all variables being dimensionless) is given by

$$m\frac{\mathrm{d}^2 x}{\mathrm{d}t^2} + \gamma\frac{\mathrm{d}x}{\mathrm{d}t} + kx = A_1\cos(\omega t + \varphi_1) + A_2\cos(\omega t + \varphi_2) \qquad (5)$$

(see Appendix B for more detail of this spring model). Analogous to the GoM O1 tidal response discussed above, the change in energy of the system from one forcing function only (take $A_2 = 0$, analogous to OB forcing) to both forcing functions (A_1 and A_2 nonzero), scaled by the energy of the system when $A_1 = 0$ (analogous to LTP forcing), is given by

$$\frac{E_{\mathrm{tot}} - E_{\mathrm{tot}}\big|_{A_2=0}}{E_{\mathrm{tot}}\big|_{A_1=0}} = 1 + 2\frac{A_1}{A_2}\cos\delta\varphi. \qquad (6)$$

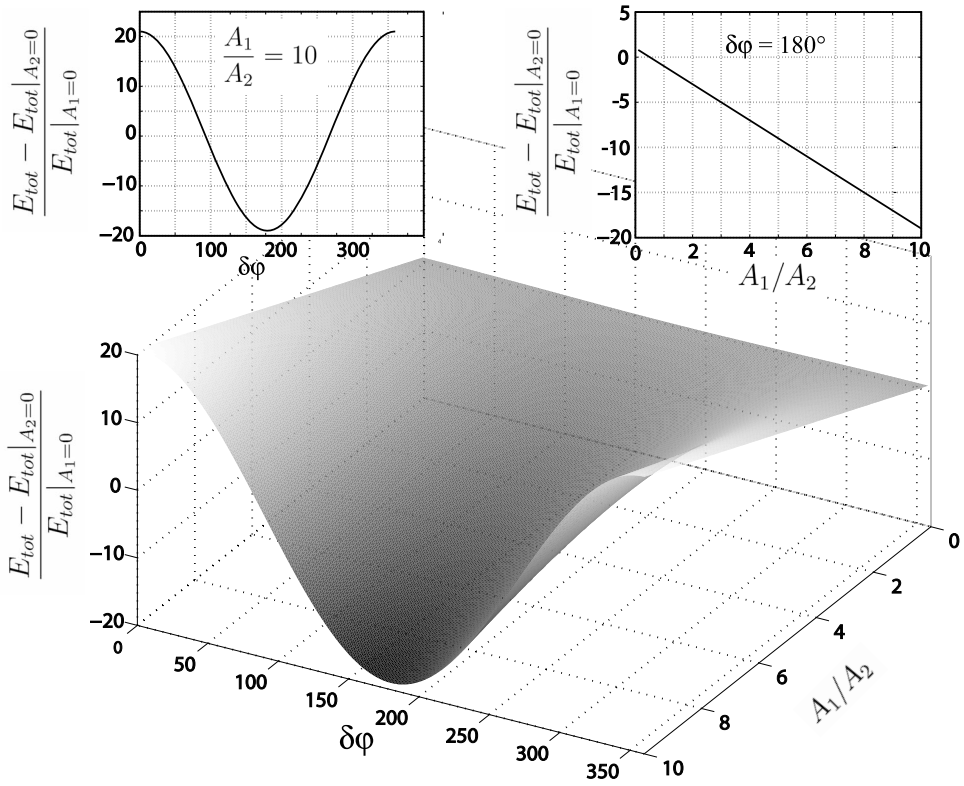

Figure 9. Solution of the spring system model (i.e., scaled total energy in the system) as a function of $\delta\phi$ and the forcing amplitude ratio.

In the case of the GoM forced by the diurnal tide, the change in energy from forcing by OB only to forcing by both OB and LTP is more than 20 times the energy in the system when forced by LTP forcing alone. In this analogous spring-mass system example, a comparable measure is simply related to the ratio of the forcing amplitudes (A_1/A_2) and the cosine of the difference in phase ($\delta\varphi$) of the forcing (equation (6)), accounting for destructive interference of the external forces (Figure 9). The change in energy in the system (6) has a nonlinear response to the phase difference but is linear to the ratio of the amplitudes of the forcing. This nonlinearity with respect to the phase difference (interference) is consistent with the nonlinearity seen in the GoM tidal response. For illustration and comparison to the case of O_1 tides described above, consider the case when a second forcing function with one tenth the amplitude of the first (A_1/A_2 = 10) and out of phase by 180° is added to a spring-mass system. The energy in the system decreases by nearly 19 times the energy when forced by the second oscillating function alone (upper frames in Figure 9).

4.2. Tidal Energy Budget

[33] For an ocean in equilibrium, forced only by a single tidal frequency, the tidally averaged energy change in the system is zero (i.e., the total energy in the system neither decreases nor increases between different tidal cycles). The energy budget is written as

$$E_f + \Delta E_l - \Gamma + \varepsilon = 0, \quad (7)$$

where E_f represent the net energy flux coming from the entrances (YC and SoF), ΔE_l is the change of energy due to local forcing (destructive/constructive interferences), Γ is the dissipation by bottom friction, and ε is the internal dissipation by numerical viscosity, the parameterized eddy viscosity, or other mechanisms, such as internal wave generation, that are not accounted for in these numerical experiments.

4.2.1. Tidal Energy Fluxes

[34] The tidal energy fluxes for each constituent are computed as [*Kowalik and Proshutinsky*, 1993]

$$\vec{F} = \left\{\rho u D\left(0.5\left(u^2 + v^2\right) + g\eta\right), \rho v D\left(0.5\left(u^2 + v^2\right) + g\eta\right)\right\}. \quad (8)$$

The time-dependent fluxes are averaged over the tidal period for the respective constituent. Equation (8) represents the energy that is transported across a unit width. By integrating energy fluxes over the width of YC and FS (Table 4), the net tidal energy flux into the GoM through the straits is computed for each experiment (Table 4) and, when divided by the tidal period, yields the average rate at which energy is lost (either through dissipation or interference) over a tidal cycle (in GJ/s, which is equivalent to GW) within the basin. A positive energy flux through the straits to the GoM indicates that the basin is a sink of tidal energy. With only the OB forcing, the only sink of energy in these experiments is dissipation through bottom friction, and this can be inferred by the energy fluxes at the straits. The average energy flux into the GoM for the M_2 tide when forced only at the OB is 1.44 GW. When both forcing mechanisms are considered,

Table 4. Average Energy Flux Rates Into the Gulf of Mexico Through the Yucatan Channel and Straits of Florida Estimated by *Reid and Whitaker* [1981] and This Study[a]

Tidal Constituent	*Reid and Whitaker* [1981]	This study LTP and OB|OB|LTP
M_2	1.3	2.45|1.44|-0.52
O_1	0.5	0.72|0.29|-0.04

[a]For the LTP, the OB, and the LTP and OB experiments.

the net rate at which M_2 tidal energy enters the GoM (and therefore is lost within the basin) is 2.45 GW. In their study, Reid and Whitaker calculated a net flux of semidiurnal tidal energy into the GoM of 1.3 GW, roughly an order of magnitude less than estimates by *Zetler and Hansen* [1971] and *Miller* [1966]. The discrepancies between the net energy dissipation in the GoM for the semidiurnal constituent calculated in this study (i.e., 2.45 GW) and from the Reid and Whitaker (1.3 GW) study could be easily explained by the different resolution of the models but also may be due to the different boundaries for the model domain. In their study Reid and Whitaker also employed an inverse modeling method and tuned their model at the ports to fit observations. They claim that their study was very sensitive to the prescribed amplitudes and phases at the ports, which in turn change the tidal energy flux through the ports. In this study, energy fluxes at the ports (SoF and YC) are much higher than estimates made by Reid and Whitaker. However, it seems that the net semidiurnal tidal energy fluxes (Table 4) for both constituents are of the same order. Energy fluxes at the SoF calculated by *Blanton et al.* [2004] are consistent with the tidal energy fluxes calculated from the experiments used in this study.

[35] The O_1 energy fluxes at both the SoF and YC are directed into the basin. The net tidal energy flux for the OB experiment is 0.30 GW, increasing to 0.72 GW with the addition of the LTP (Table 4). Again, these estimates are of comparable magnitudes to estimates by Reid and Whitaker. The increased tidal energy flux (and therefore rate at which energy is lost in the GoM) with the addition of the LTP may be due to destructive interference, also suggested by a weakening of the tidal amplitudes at the coastal stations around the GoM (Figure 7).

4.2.2. Tidal Energy Dissipation

[36] The only source of dissipation of tidal energy in the OB experiment is bottom friction (assuming negligible contribution from horizontal friction), whereas in the LTP and OB experiment, the LTP forcing can also act like a source or sink of tidal energy by creating destructive/constructive interferences between the free wave and the forced wave (see above section). It has been shown that an accurate expression for the mean rate of tidal energy dissipation per unit area by bottom friction from numerical simulation is [*Davies et al.*, 1985]:

$$\Psi = \frac{1}{T} c_b \rho \int_0^T \left(u^2 + v^2\right)^{3/2} dt, \tag{9}$$

where T is the period of the tidal constituent considered, c_b the drag coefficient, and u and v are components of the tidal velocities. For the M_2 tide, this results in values of 0.01–0.33 W m^{-2} at the WFS, Louisiana-Texas shelf, and Campeche Bank regions, and is highest near the Florida Keys and the Florida Big Bend region for the LTP and OB experiment (not shown). For the OB experiment, the region of dissipation is the same but with somewhat smaller values ranging from 0.01 W m^{-2} to 0.19 W m^{-2}. The tidal dissipation is small (<0.01 W m^{-2}) everywhere else, especially in the deep ocean where tidal velocities are very weak. For the O_1 tide, the tidal dissipation values range from 0.01 to 0.08 W m^{-2} at the WFS, Louisiana-Texas Shelf, and Campeche Bank for both the OB and LTP and OB experiments. The diurnal tide energy dissipation is in general weaker but takes place on all the wide shelves of the GoM, while the semidiurnal tidal dissipation by bottom friction dominantly occurs at the WFS. *Blanton et al.* [2004] have stated that in estuaries tidal dissipation rates are typically 0.5 W m^{-2}, larger than over the shelf, which is comparable to our findings.

[37] The mean rate of tidal energy dissipation per unit area by bottom friction is now integrated over the GOM domain (solid white line in Figure 1) for the OB experiment to demonstrate that the tidal energy budget is nearly closed for this specific experiment (i.e., bottom friction dominates over numerical or parameterized viscosity). For the M_2 tidal constituent, 1.26 GW is dissipated while there is 0.29 GW dissipated for O_1. This agrees (excepting for numerical integration errors) with the average energy dissipation rates calculated from energy fluxes through the YC and SoF (Table 4) and clearly illustrates that the energy budget is closed when only the bottom friction dissipation mechanism is present in the numerical simulations.

4.2.3. Tidal Energy Budget Discussion

[38] This study is intended to yield new insight into the behavior of tides in the GoM, but care must be taken when interpreting the results and one needs to understand the limitations of the numerical experiments. As previously mentioned, parameterization and simulation of the effects of bottom friction are important for the dissipation of tidal energy. The overall rate of tidal energy dissipation due to bottom friction dominates that due to horizontal friction [*Kowalik and Polyakov*, 1998]. Tidal energy dissipation due to bottom friction is proportional to $\tau_b \overline{\mathbf{u}}$ [*Brown and Trask*, 1980], where τ_b is the bottom stress and $\overline{\mathbf{u}}$ is the vertically averaged horizontal velocity. In the model, this bottom friction is given by a quadratic rule where the bottom drag coefficient becomes constant for depths below 17 m. The Reid and Whitaker study shows that, by simple tuning, the bottom friction is crucial for simulating tidal dissipation patterns in the GoM as the semidiurnal tide phases are very sensitive to this parameter (the amphidromic point location is particularly sensitive). It is likely that in shallow waters the simple parameterization of bottom drag by using a spatially constant typical bottom roughness scale height of 3 mm is not sufficient for accurately modeling the local tidal dissipation.

[39] A study by *Blanton et al*. [2004] also demonstrates the importance of resolving inlets and estuaries in a regional model for simulating tides. *Blanton et al*. [2004] show that resolving these shallow regions improves the representation of the cross-shelf amplification as well as the phases for the semidiurnal tides in a model of the South Atlantic Bight.

Similar coastal features are not well resolved in the GoM numerical model configuration used for this study, and this may lead to inaccuracies in the simulation of tidal dissipation.

[40] This study has used barotropic simulations that necessarily neglect the conversion from barotropic to baroclinic tides, which will act as a sink of energy. Although, in theory, internal tides play an important role in the deep ocean mixing and contribute to the tidal energy dissipation [*Munk and Wunsch*, 1998], this may not be true for every region. Over a flat-bottom ocean basin, no internal tides can be generated [*Morozov*, 1995; *Kantha and Clayson*, 2000]; thus, no dissipation through baroclinic tides is anticipated in such a region. The deep GoM is relatively flat so one should expect only weak generation of internal tides here, and the application of a barotropic model is reasonably appropriate for this study focusing on tides over the basin scale. Over the margins of the continental shelf regions, baroclinic tides may dissipate as much as 15% of the barotropic tidal energy [*Kantha and Tierney*, 1997]. It is noteworthy that baroclinic tides are concentrated around the topographic irregularities and quickly dissipate as they propagate away from their source. Thus, it is anticipated that most of the internal tide energy is concentrated only in the immediate vicinity of the steep topographic features [*Wunsch*, 1975; *Kantha and Clayson*, 2000]. The outer WFS and the YC are the only regions in this domain where significant internal wave activity has been recorded [*Rubenstein*, 1999] and where the tidal conversion could have an effective impact on the model tidal solution.

[41] It is also important to note that since the bottom drag owing to tidal motions from different tidal constituents is not linearly separative, the experiments conducted with only one tidal constituent (section 4) produce a different bottom drag from the experiment conducted with all tidal constituents (section 3). Although it might change the wave propagation (i.e., tidal phase), this impact is negligible (as evidenced by comparison of the tidal phases and amplitudes of the experiments forced with four tidal constituents versus the experiments forced by only a single constituent) and is not considered in this study.

5. Summary and Conclusions

[42] A high-resolution model has been configured to simulate and study barotropic tides in the GoM region. Three model experiments have been run by applying different forcing to the model: (1) only local tidal potential forcing within the domain, (2) only the barotropic tidal signal prescribed at the model open boundaries, and (3) both forcing mechanisms combined. Results show that the LTP acts to modify the semidiurnal tides propagating through the straits connecting the GoM to the Atlantic and Caribbean and is crucial for accurate simulation of the M_2 and S_2 tides. The LTP has less impact on the diurnal tides in the GoM, which are mainly due to resonance of the basin with the diurnal tidal oscillations of the western Atlantic.

[43] The simulated major semidiurnal and diurnal tidal constituents (M_2, S_2, O_1, and K_1) are compared with observations at several stations in the GoM. The most realistic experiment (LTP and OB) agrees with previous model results [*Kantha*, 2005; *Mukai et al.*, 2002] and observations of the principal diurnal and semidiurnal tidal constituent amplitudes and phases in the GoM. Accurate simulation of the semidiurnal tides in the GoM requires both LTP and OB forcing. When LTP is omitted, reasonable tidal amplitudes are simulated but phase errors are typically 30°–40°. Phase errors are improved with the addition of LTP. This local body forcing acts to slow the apparent tidal wave propagation through the central GoM. Phases for the diurnal tidal constituents are well simulated with just OB forcing, but the amplitudes are somewhat overestimated. Slight modification of the tidal wave by LTP decreases the diurnal tidal amplitudes so that they more closely match observations.

[44] Calculations of LTP and OB forcing to the tidal energy in the GoM for O_1 and M_2 show that their contributions are not linearly additive. OB forcing supplies a freely propagating (except for frictional dissipation) tidal wave throughout the basin. The addition of the LTP forcing constructively or destructively interferes with the OB forced tide, depending on the phase difference between the OB and LTP forcing. For the O_1 tide, addition of the LTP forcing to the OB-forced tide acts to reduce the total tidal energy in the GoM by roughly 20 times the total energy contributed by LTP forcing alone. This nonlinearity is illustrated analytically by a forced mass-spring system.

[45] The tidal energy budget is diagnosed for the O_1 and M_2 tidal constituents. For both semidiurnal and diurnal constituents, the net energy flux through the straits is of similar magnitude to estimates from previous studies. Tidal fluxes and tidal energy dissipation computations in the GoM highlight the importance of shelf regions for tidal dissipation. Maps of tidal energy density for the experiments show clearly the amplification of the tidal oscillations across these wide shelves of the GoM. Ratios of the energy density for experiments with different forcing mechanisms show regions where constructive or destructive interference of the tidal signal by LTP occurs.

[46] Finally, the model results yield a new estimate of tidal amplitudes and phases within the GoM. The approach of using a suite of numerical experiments to isolate the remote tidal signal (OB) and locally forced tide (LTP) allows investigation of the interaction between them within the GoM. These results may be applied to improve the simulation of tides in other semienclosed seas.

Appendix A: Linear Regression Model and Studentized Residual Test

[47] To quantify the relation between the modeled and observed amplitudes a fitted linear regression model is applied

$$y_i = \alpha + \beta x_i + e_i, \tag{A1}$$

where y and x are simulated and observed tidal amplitudes (respectively) at station i and e is the random error under the standard normality assumption (uncorrelated and normally distributed $\sim N(0, \sigma^2)$). The outliers are identified based on Studentized residual analysis [*Hoaglin and Welsch*, 1978; *Jennrich*, 1995]. For the simple linear regression model (A1), outlier points indicate locations where simulated tidal amplitudes have no (significant) linear relation with observed values; i.e., they do not correlate well. The Studentized residual analysis is a valuable statistical tool to

objectively identify those locations where the model badly matches observations.

[48] The Studentized residual is defined as

$$r_i = \frac{\hat{e}_i}{\hat{\sigma}(1-h_{ii})^{1/2}}, \tag{A2}$$

where $\hat{e}_i$ are the fitted residuals and $\hat{\sigma}$ is the square root of the residual mean square:

$$\hat{\sigma}^2 = \frac{\sum_{i=1}^{n} \hat{e}_i^2}{n-2}. \tag{A3}$$

The residual mean square is an unbiased estimate of σ^2 the variance of the error term in (A1). In (A2), h_{ii} is the leverage of the ith observation that is defined as

$$h_{ii} = \mathbf{x}_i \left(\mathbf{X}'\mathbf{X}\right)^{-1} \mathbf{x}_i', \tag{A4}$$

where $\mathbf{X}$ is the matrix of carriers (or design matrix), and $\mathbf{x}_i = (x_{i1}, \ldots, x_{ip})$ denotes the ith row of $\mathbf{X}$. The leverage quantifies the effect on the vector of fitted responses $\overline{\mathbf{y}}$ of changing the ith observation by 1 unit. Those observations that strongly affect the regression line by a 1 unit change have high leverage (they are not necessarily outliers).

[49] A large value of $\hat{e}_i$, and thus r_i, suggests that the ith observation is an outlier. r_i does not have a t distribution. Instead, the squared externally Studentized residual is calculated based on r_i

$$t_i^2 = \frac{n-p-1}{n-p} \frac{r_i^2}{1-r_i^2/(n-p)}, \tag{A5}$$

where n is the number of data values and p is the number of estimated parameters in a regression model. For the case considered in this paper, $n = 62$ (number of tidal stations), $p = 2$, and t_i has a Student's t distribution with $(n\text{-}p\text{-}1)$ degrees of freedom. Values of t_i greater than $t_{0.025}(59) = 2$ correspond to the observations that can be considered outliers at the 0.05 significance level.

Appendix B: Description of the Mass-Spring Model

[50] Tidal motions in the GoM are damped forced oscillations that can be approximated by a mechanistic model of a mass-spring system. The model and its solutions are discussed in many texts on ordinary differential equations. Here major steps to solving this problem are outlined.

[51] The model consists of a spring with spring constant k, damping constant (friction) γ, and a body of mass m attached to the spring. There are two external periodic forces acting on the body representing LTP and OB forcing. The model of this system is

$$m\frac{\mathrm{d}^2x}{\mathrm{d}t^2} + \gamma\frac{\mathrm{d}x}{\mathrm{d}t} + kx = A_1\cos(\omega t + \varphi_1) + A_2\cos(\omega t + \varphi_2), \tag{B1}$$

where A_1 and A_2 are amplitudes of the forces acting on the body, ω is the frequency of the forces, and ϕ_1 and ϕ_2 are phase shifts. The right-hand side is rearranged as

$$A\cos(\omega t - \theta), \tag{B2}$$

where

$$A = \sqrt{A_1^2 + A_2^2 + 2A_1A_2\cos(\phi_1 - \phi_2)}, \tag{B3}$$

$$\theta = \tan^{-1}\left(\frac{A_1\sin\phi_1 + A_2\sin\phi_2}{A_1\cos\phi_1 + A_2\cos\phi_2}\right), \tag{B4}$$

resulting in the equation

$$m\frac{\mathrm{d}^2x}{\mathrm{d}t^2} + \gamma\frac{\mathrm{d}x}{\mathrm{d}t} + kx = A\cos(\omega t + \theta), \tag{B5}$$

which can be readily solved [*Kreyszig*, 1999].

[52] Because the system has friction, the transient solution of (B5) approaches the steady state solution

$$y_p = C\cos(\omega\tilde{t} - \eta), \tag{B5A}$$

where $\omega\,\tilde{t} = \omega t - \theta$, and $\tan\eta = \frac{\omega\gamma}{m\left(\omega_0^2-\omega^2\right)}$. $\omega_0 = \sqrt{k/m}$ is the fundamental frequency of the system. The amplitude C of the steady state solution is

$$C = \frac{A}{\sqrt{m^2\left(\omega_0^2-\omega^2\right)^2 + \omega^2\gamma^2}}. \tag{B5B}$$

For simplicity, and without loss of generality, it is further assumed that the system has a unit mass. Then the total energy (kinetic plus potential energy) of this system, integrated over a period $2\pi\ \omega^{-1}$, is given by

$$E_{\mathrm{tot}} = \frac{\left(\omega^2+\omega_0^2\right)\left(A_1^2 + A_2^2 + 2A_1A_2\cos(\delta\varphi)\right)}{4\left(\gamma^2\omega^2 + \left(\omega^2-\omega_0^2\right)^2\right)}, \tag{B6}$$

where $\delta\phi$ is phase difference between the forcing terms.

[53] **Acknowledgments.** This research was funded by the Office of Naval Research through a Secretary of the Navy grant awarded to James J. O'Brien and by a NASA Office of Earth Science grant. We also thank the Florida State University and the NOAA sponsored Northern Gulf of Mexico Cooperative Institute for providing the observational data from the K Tower station.

References

Arbic, B. K., and C. Garrett (2009), A coupled oscillator model of shelf and ocean tides, *Cont. Shelf. Res.*, doi:10.1016/j.csr.2009.07.008.

Asselin, R. (1972), Frequency filter for time integrations, *Mon. Weather Rev.*, *100*, 487–490.

Blanton, B. O., F. E. Werner, H. E. Seim, R. A. Luettich Jr., D. R. Lynch, K. W. Smith, G. Voulgaris, F. M. Bingham, and F. Way (2004), Barotropic tides in the South Atlantic Bight, *J. Geophys. Res.*, *109*, C12024, doi:10.1029/2004JC002455.

Brown, W. S., and R. P. Trask (1980), A study of tidal energy dissipation and bottom stress in an estuary, *J. Phys. Oceanogr.*, *10*, 1742–1754.

Clarke, A. J. (1995), Northeastern Gulf of Mexico physical oceanography workshop; proceedings of a workshop held in Tallahassee, Florida, 5–7 April 1994, Florida State University, OCS Study MMS 94-0044. U. S. Department of the Interior, Minerals Management Services, Gulf of Mexico OCS Region, New Orleans, La. 257pp.

Clarke, A. J., and D. S. Battisti (1981), The effect of continental shelves on tides, *Deep Sea Res.*, *28*, 665–682.

Davies, A. M., J. Sauvel, and J. Evans (1985), Computing near coastal tide dynamics from observations and a numerical model, *Cont. Shelf Res.*, *4*, 341–366.

Flather, R. A. (1976), A tidal model of the northwest European continental shelf. Memoires de la societe, *Royale de Liege*, *6*(10), 141–162.

Grace, S. F. (1932), The principle diurnal constituent of tidal motion in the Gulf of Mexico, *Mon. Not. R. Astron. Soc.*, *3*, 70–83.
Grijalva, N. (1971), The M2 tide in the Gulf of Mexico, *Geofis. Int.*, *11*(3), 103–125.
Henson, J. I., F. Muller-Karger, D. Wilson, S. L. Morey, G. A. Maul, M. Luther, and C. Kranenburg (2006), Strategic geographic positioning of sea level gauges to aid in early detection of tsunamis in the intra-Americas Sea, *Sci. Tsunami Hazards*, *25*(3),173–207.
He, R., and R. H. Weisberg (2002), Tides on the West Florida shelf, *J. Phys. Oceanogr.*, *32*, 3455–3473.
Hoaglin, D. C., and R. E. Welsch (1978), The hat matrix in regression and ANOVA author(s), *Am. Stat.*, *32*(1), 17–22.
Jammalamadaka, S. R., and Y. R. Sarma (1988), A correlation coefficient for angular variables, in *Statistical Theory and Data Analysis II. North Holland, Amsterdam*, edited by K. Matusita, 349–364.
Jennrich, R. I. (1995), An Introduction to Computational Statistics: Regression Analysis, Prentice-Hall, Englewood Cliffs, NJ.
Kantha, L. (2005), Barotropic tides in the Gulf of Mexico, in *Circulation of the Gulf of Mexico: Observations and Models*, 347, Wilton Sturges and Alexis Lugo-Fernandez.
Kantha, L., and C. A. Clayson (2000), Numerical Models of Oceans and Oceanic Processes, *Int. Geophys. Ser.*, *66*, Academic.
Kantha, L. H., and C. C. Tierney (1997), Global baroclinic tides, *Progr. Oceanogr.*, *40*, 163–178.
Kowalik, K., and I. Polyakov (1998), Tides in the Sea of Okhotsk, *J. Phys. Oceanogr.*, *28*, 1389–1409.
Kowalik, K., and A. Y. Proshutinsky (1993), Diurnal tides in the Arctic Ocean, *J. Geophys. Res.*, *98*(C9), 16,449–16,468, doi:10.1029/93JC01363.
Kreyszig, E. (1999), Advanced Engineering Mathematics, 1154 pp., New York.
Le Provost, C., F. Lyard, J. M. Molines, M. L. Genco, and F. Rabiloud (1998), A hydrodynamic ocean tide model improved by assimilating a satellite altimeter-derived data set, *J. Geophys. Res.*, *103*(C3), 5513–5529, doi:10.1029/97JC01733.
Marmer, H. A. (1954), Tides and sea level in the Gulf of Mexico, *Fish. Bull. U. S.*, *55*(89), 101–118.
Martin, P. J. (2000), A description of the Navy Coastal Ocean model Version 1.0, NRL, Rep. NRL/FR/7322-009962, 39 pp., Naval Res. Lab., Stennis Space Center, Miss.
Mellor, G. L. (1996), Introduction to Physical Oceanography, 253 pp., Springer.
Mikhailov, Y. D., V. P. Meleshko, and G. I. Shcheveleva (1969), Computation of tides and tidal currents in the Gulf of Mexico and Caribbean Sea, *Deep Sea Res.*, *24*, 987–1004.
Miller, G. R. (1966), The flux of tidal energy out of deep oceans, *J. Geophys. Res.*, *71*(10), 2485–2489, doi:10.1029/JZ071i010p02485.
Morozov, E. G. (1995), Semidiurnal internal wave global field, *Deep Sea Res., Part I*, *42*(1), 135–148.
Mukai, A. Y., J. J. Westerink, R. A. Luettich Jr., and D. Mark (2002), A tidal Constituent Database for Western North Atlantic, Gulf of Mexico, and Caribbean Sea. Eastcoast 2001. Report 194 pp.
Mungall, J. C. H., C. E. Able, and C. R. Olling (1978), Hydrodynamic model estimates of the M2 and K1 currents of the Gulf of Mexico, Ref. 78-9-T, Dept. of Oceanography, Texas A&M University.
Munk, W., and C. Wunsch (1998), Abyssal recipes II: Energetics of tidal and wind mixing, *Deep Sea Res.*, *45*, 1977–2010.
Pawlowicz, R., B. Beardsley, and S. Lentz (2002), Classical tidal harmonic analysis including error estimates in Matlab using T_Tide, *Comput. Geosci*.
Reid, R. O., and R. E. Whitaker (1981), Numerical model for astronomical tides in the Gulf of Mexico, pp. 115, Texas A&M Univ. Report for U. S. Army Engineers Waterway Experiment Station, College Station, Tex.
Rubenstein, D. (1999), Observations of cnoidal internal waves and their effect on acoustic propagation in shallow water, *J. Oceanic Eng.*, *21*(3).
Schwiderski, E. W. (1979), Global Ocean Tides, Part 2: The Semi-Diurnal Principal Lunar Tides (M2), Atlas of Tidal Charts and Maps. Naval Surface Weapons Center, Dahlgren, Va, and Silver Springs, Md, NSWDTR, 79-414.
Schwiderski, E. W. (1980), Ocean tides, Part 1 and Part 2, *Mar. Geod.*, *3*, 161–255.
Servicio del Golfo de Mexico y Mar Caribe (2007), Tablas de Prediccion de Mareas 2007, UNAM, Mexico, D.F.
Wunsch, C. (1975), Internal tides in the ocean, *Rev. Geophys.*, *13*, 167–182.
Zetler, B. D., and D. V. Hansen (1971), Tides in the Gulf of Mexico, in *Contributions on the Physical Oceanography of the Gulf of Mexico*, vol. 2, edited by L. R. A. Capurro, and J. L. Reid, Gulf, 265–275.

J. J. O'Brien, D. S. Dukhovskoy, F. Gouillon, and S. L. Morey, Center for Ocean Atmospheric Prediction Studies, Florida State University, Tallahassee, FL 32306-2840, USA. (gouillon@coaps.fsu.edu)